ARTICLE NO. 79-0643R

Prediction of the Acoustic Environment in the Space Shuttle Payload Bay

John F. Wilby* and Larry D. Pope†
Bolt Beranek and Newman Inc., Canoga Park, Calif.

An analytical model has been developed to predict space-averaged sound levels in the payload bay of the Space Shuttle when the bay is empty or when a payload is present. The model utilizes the power flow concept and takes into account net power flow from the exterior, flow between subvolumes surrounding a payload, and power dissipation in the subvolumes. The characteristics of the model are described, and its application to the Spacelab configuration 2 payload is presented to illustrate the type of results obtained.

Introduction

THE Space Shuttle orbiter vehicle (Fig. 1) introduces a new geometry for launch vehicles of spacecraft payloads, and creates new problems for payload acoustic exposure at liftoff. These problems arise because the payloads are closer to the rocket exhaust nozzles than in earlier launch vehicles, and the nozzles are more widely separated, creating a larger source volume.

Early in the design stages of the Space Shuttle, a need was identified for a reliable prediction procedure to estimate sound levels in the payload bay, with and without payload (see, for example, Ref. 1). The analytical model described in the following sections was developed in response to this need. Development of such a model requires a comprehensive program of model formulation and validation, and in the present case both model and full-scale tests have been performed during validation phases.[2]

Prediction of Vehicle Interior Noise

An analytical model for the interior acoustic environment has to provide adequate descriptions of the exterior noise field, the dynamic characteristics of the transmitting structure, and the acoustic properties of the receiving interior volume. Several studies[1,3-7] have considered the acoustic transmission problem for flight vehicles. However, few of the studies actually attempted to validate the analytical model with known experimental data, and the only attempt[3] in the referenced studies mentioned previously shows a discrepancy of 15-20 dB between prediction and measurement. It is evident that a prediction procedure for the acoustic environment in the payload bay of the Space Shuttle orbiter vehicle has to undergo a fairly intensive validation process before it can be accepted as a reliable method.

The prediction methods identified in the preceding paragraph[1,3-7] use several different approaches in the formulation of the analytical model. Hay[3] follows an essentially empirical approach, combining model and full scale data for the exterior pressure field and structural response with simple calculations based mainly on mass-law transmission theory. Early predictions by On[1] for the Space Shuttle also used mass-law transmission theory with modifications at low frequencies to account for structural stiffness effects. The statistical energy analysis method was used by Wilby and Scharton[5] for what was mainly a high-frequency transmission study, whereas Cockburn and Jolly[4] based their analysis on the calculation of structural joint acceptance functions for a cylindrical fuselage and the coupling of the structural modes with those of the cylindrical volume. Cylindrical structures are also considered by Koval in a series of papers, of which the two references listed[6,7] constitute the more recent developments.

The studies identified previously contain various deficiencies which make them unsuitable for application to the Space Shuttle. Most of the methods do not adequately represent both the low- and high-frequency regimes of interest to the Space Shuttle payload environment. Furthermore, many of the methods mentioned earlier are concerned with simple cylindrical volumes rather than the complicated shapes which occur around payloads. Finally, none of the methods addresses the problem of acoustic interaction between connected subvolumes.

General Approach

The basic approach followed in the development of the analytical model of the acoustic environment in the payload bay of the Space Shuttle is that of power balance. This is achieved by equating the net power flow into a volume to the power dissipated within that volume. When a payload is present, the single cavity formed by the empty bay is broken up into a series of interconnecting subvolumes which surround the payload (Fig. 2). In this case, the acoustic power flow between subvolumes has to be included in the power balance equations.

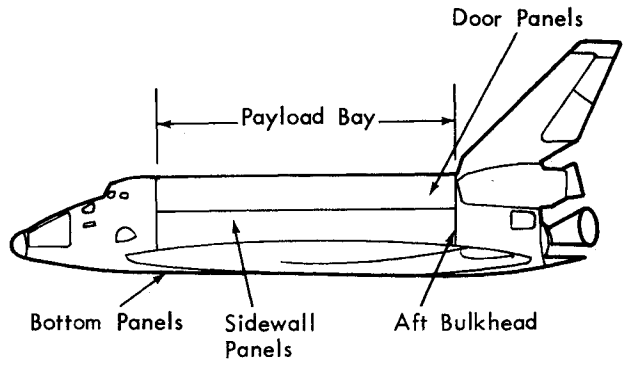

Fig. 1 Space Shuttle orbiter vehicle showing mid-fuselage structure.

Presented as Paper 79-0643 at the AIAA 5th Aeroacoustics Conference, Seattle, Wash., March 12-14, 1979; submitted April 17, 1979; revision received Oct. 5, 1979.

Index categories: Noise; Spacecraft Configurational and Structural Design (including Loads).

*Senior Scientist. Associate Fellow AIAA.
†Senior Scientist.

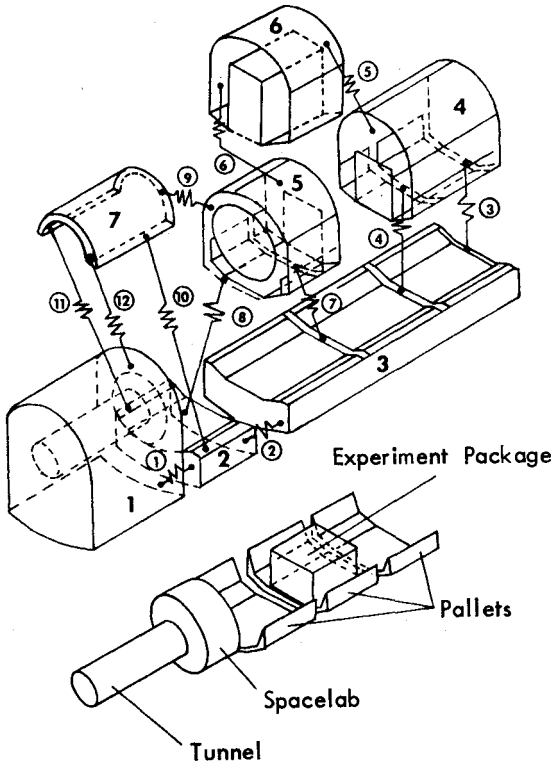

Fig. 2 Spacelab configuration 2 idealization.

An outline of the power flow approach can be obtained from the following generalized matrix equation. The power flow equation can be written, for each frequency band, as

$$\{W\} = [C]\{P\} \tag{1}$$

where $\{W\}$ is the inflow power vector, $[C]$ is a coupling matrix, and $\{P\}$ is a column of space-averaged mean-square pressures in the subvolumes. The dimension of Eq. (1) is equal to the number of subvolumes in the bay.

Vector $\{W\}$ has elements

$$W(K) = \sum_J W(K,J)$$

where K is a subvolume identifier and J a structure identifier. Coupling matrix $[C]$ has diagonal elements $C(K,K)$ and off-diagonal elements $C(K,I)$, where I is also a subvolume identifier. The equation for $C(K,K)$ can be written

$$C(K,K) = C_\alpha(K,K) + C_p(K,K) + \sum_J C_J(K,K) + \sum_L C_L(K,K) \tag{2}$$

where $C_\alpha(K,K)$ and $C_p(K,K)$ represent power absorption on, respectively, bounding surfaces of the subvolume and payload surfaces in the subvolume, which are not bounding surfaces. $C_J(K,K)$ represents outward transmission of power through structure J, and $C_L(K,K)$ gives transmission through opening L to a coupled subvolume. Power flow through opening L into subvolume K from adjacent subvolume I is given by

$$C(K,I) = \sum_L C_L(K,I) \tag{3}$$

Development of the power flow equations which define $W(K,J)$ and $C_J(K,K)$ is presented in Refs. 8 and 9, and the results are directly applicable to this model for the Space Shuttle. The equations in Ref. 8 refer to power flow to resonant acoustic modes of the cavity, via resonant and nonresonant (mass-controlled) modes of the structure. Resonance implies that a mode has its resonance frequency within the frequency band of interest. The analysis is extended in Ref. 9 to include nonresonant response of the cavity. Results for the power inflow relations are presented in the Appendix. The expressions presented encompass the modal approach at low frequencies and a form of statistical energy analysis at high frequencies.

Several assumptions are introduced in the development of the power balance equations in order to achieve a prediction method which can be applied to a practical situation such as the Space Shuttle. The transmitting structure of the orbiter vehicle is assumed to cover a cavity which has sound-absorbing surfaces on the walls. The cavity, whether it be the empty bay or a subvolume surrounding a payload, is assumed to be basically rectangular, but curvature of the walls can be taken into account. In general, each subvolume is assumed to have reflecting boundaries which can support acoustic modal systems, although there can be some exceptions.

The model also assumes that the coupling between the structure and cavity is "weak." This is a common assumption when the fluid in the cavity is gaseous and when there are likely to be leaks. The assumption permits the coupling to be calculated using in vacuo resonance frequencies of the structure and blocked, or rigid wall, response of the cavity. Thus, the power flow between a given mode of the structure and a mode of the cavity can be evaluated without including the interaction of any other mode. It should be noted that the assumption of "weak coupling" does not exclude "well-coupled" modes. Well-coupled acoustic and structural modes are those modes that have closely spaced resonance frequencies, and modal pairs of this type are included in the analytical model.

Structural Response

The Appendix shows that the power inflow depends on the exterior jet noise field through the joint acceptance function

$$j^2_{MN}(\omega) = \frac{1}{A^2 S_p(\omega)} \int_A S_p(x,x',\omega)\psi_{MN}(x)\psi_{MN}(x')\,dx\,dx'$$

where A is the panel area, $S_p(\omega)$ the blocked pressure power spectral density for the exterior pressure field, $S_p(x,x',\omega)$ the blocked cross power spectral density function, and $\psi_{MN}(x)$ the mode shape function for modes of order (M,N). For Space Shuttle calculations, $S_p(\omega)$ is obtained from measurements made on a 6.4% scale model.[10,11] Only the real part of the cross power spectral density is required, and this is written as

$$\mathrm{Re}[S_p(x,x',\omega)] = S_p(\omega)\rho(x,x',\omega)$$

where

$$\rho(x,x',\omega) = \rho(\xi,\omega) = \rho_x(\xi,\omega)\rho_y(\zeta,\omega)$$

and

$$\xi = x' - x$$

The correlation functions are assumed to have the form associated with a convected pressure field

$$\rho_x(\xi,\omega) = \exp[-k_x|\xi|/a_x]\cos(k_x\xi)$$

with a similar expression for $\rho_y(\zeta,\omega)$. From Ref. 11,

$$k_x = 0.9k \qquad a_x = 31$$

$$k_y = 0.382k \qquad a_y = 3.2$$

where wavenumber $k=\omega/c$, and c is the speed of sound.

The structural components are assumed to be supported at major junctions (discontinuities) with mode shapes assumed to be of the form

$$\psi_{MN}(x) = \sin k_M x \sin k_N y$$

at frequencies where such representations seem adequate.

The payload bay structure is idealized as a series of equivalent flat or curved orthotropic panels. The panels are derived by distributing the bending rigidity of stringers and frames uniformly over the associated panel surfaces. Resonance frequencies for the orthotropic panels are calculated, to a first approximation, using equations given in Ref. 11, but at low frequencies, adjustments are made to bring the resonance frequencies into closer agreement with values calculated using more detailed finite-element analysis.[11]

The analytical model divides the payload bay structure into six regions: payload bay door, fore and aft sidewall, fore and aft bottom panels, and aft bulkhead. These regions are identified in Figs. 1 and 3. The sidewall and bottom structures are each divided into fore and aft regions because of differences in structural construction and exterior pressure levels. Joint acceptances calculated for the structural regions are shown in Figs. 4 and 5. Figure 4 shows that the joint acceptance spectrum for the door is constructed from values calculated from stiffened and unstiffened door models. This representation was adopted following analysis of data from validation tests.

Modal density spectra are also calculated for the payload bay structures, and the results are given in Fig. 6. It can be seen in Figs. 5 and 6 that the curves for some structural regions do not extend to low frequencies. This is because a simple low-frequency representation for the sidewall is deemed inadequate, and is therefore not in the analytical model, and because the low-frequency representation for the bottom structure, which utilized data provided by modal analysis,[11] is excluded from the figures.

Damping loss factors for the structures are obtained from published empirical data for similar structures. A review of available data is presented in Ref. 11, and Fig. 7 shows data

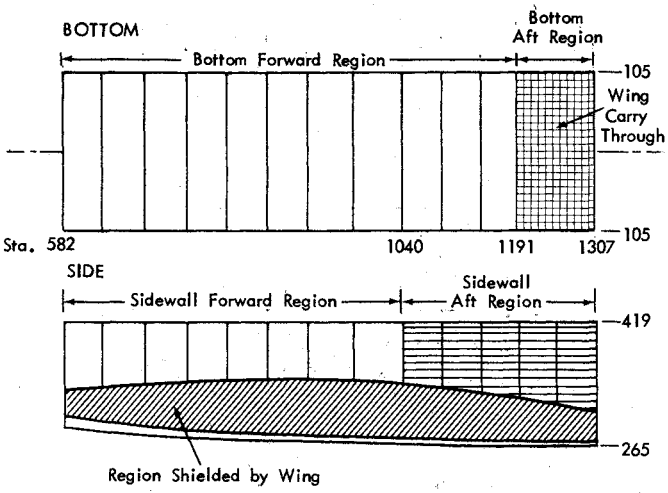

Fig. 3 Bottom and sidewall of payload bay, showing separate regions used in analytical model.

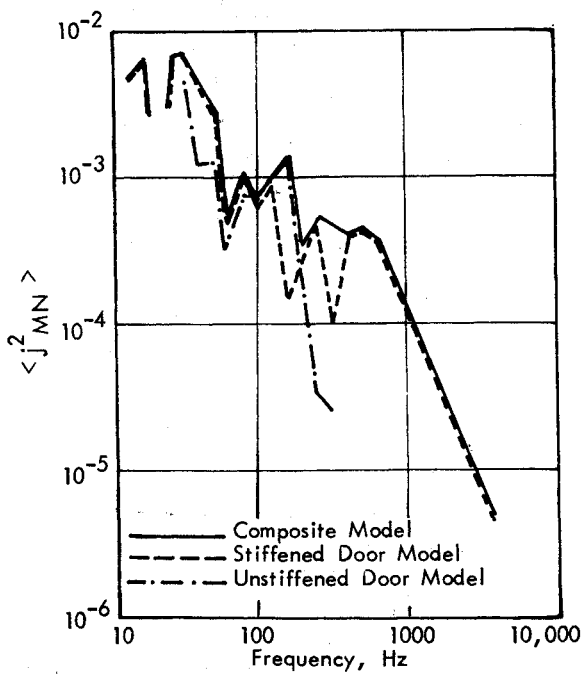

Fig. 4 Band average joint acceptance for payload bay door (one-third octave band).

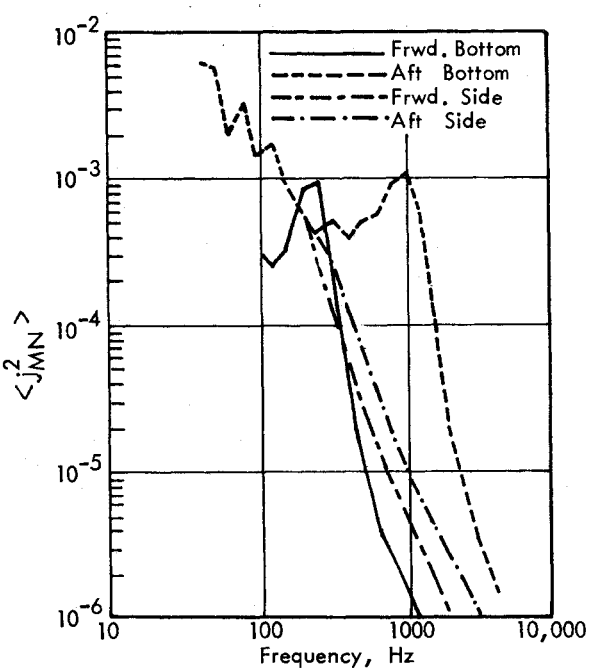

Fig. 5 Band average joint acceptance for structure (one-third octave band).

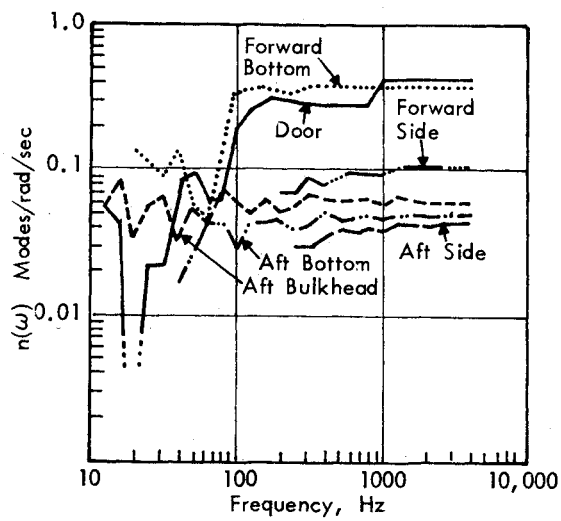

Fig. 6 Calculated modal densities for payload bay structure.

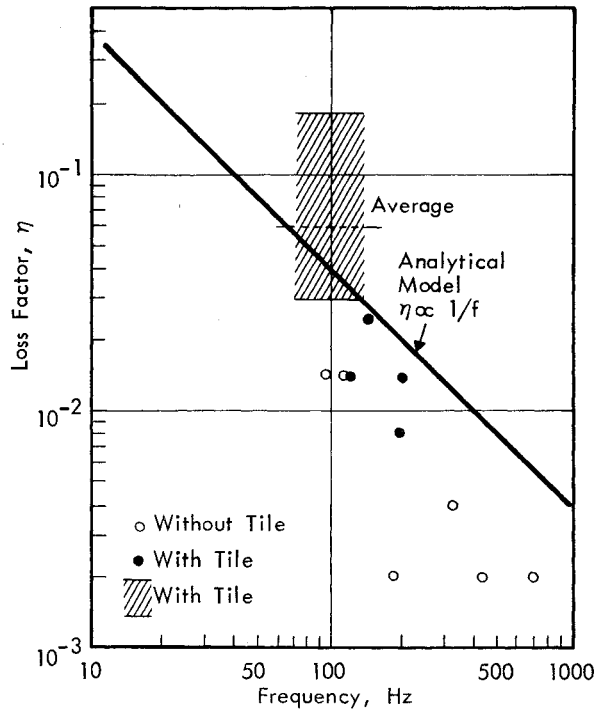

Fig. 7 Damping of aluminum test structures with thermal protection system tiles.

for aluminum structures with thermal protection system tiles such as those used on the Space Shuttle. The loss factor model assumed for the aluminum structure is $\eta = 4/f$ where f is the frequency, and for the payload bay door, which is of honeycomb construction with graphite/epoxy components, $\eta = 2/f$. The assumed model is shown in Fig. 7.

Cavity Response

The acoustic power flowing into a volume or subvolume is determined at low frequencies by the coupling between the modes of the structure and the cavity. This coupling is defined in terms of the function

$$f(n,r) = \frac{1}{A_i}\int_{A_i} \phi_n(x)\psi_r(x)\,dx = f_x(p,M)f_y(q,N) \qquad (4)$$

where A_i is the area of the radiating structure and $\phi_n(x)$ is the cavity mode shape. At high frequencies, where there are many structural and acoustic modes in a given frequency bandwidth, the coupling can be expressed more conveniently in terms of the radiation efficiency, values of which are plotted in Fig. 8.

In order to calculate resonance frequencies and mode shapes for the empty payload bay or a subvolume, it is assumed that the cavity has a basic rectangular parallelepiped shape with one or more curved boundaries. The influence of the curved boundaries is included by means of a perturbation-type approach[11] applied to the basic solution to the Helmholtz equation

$$\nabla^2\phi + k^2\phi = 0$$

with boundary condition $\boldsymbol{n}\cdot\nabla\phi = 0$, where $\boldsymbol{n}$ is the normal to the surface. The perturbation approach assumes that the deformation due to curvature is small relative to the dimensions of the cavity (e.g., in Fig. 9, $R/b \ll 1$).

For the case shown in Fig. 9, the eigenvalue for mode pqr of the deformed parallelepiped is given by

$$k_{pqr} = k^{\circ}_{pqr}\left\{1 + \frac{2R\gamma_{pq}}{b}\left[\left(\frac{p\pi}{a}\right)^2 + \left(\frac{q\pi}{b}\right)^2\right](k^{\circ}_{pqr})^{-2}\right\}^{1/2}$$

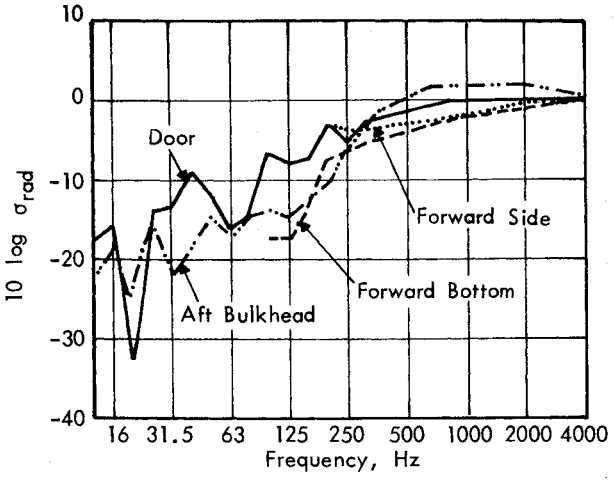

Fig. 8 Calculated radiation efficiencies for payload bay structures.

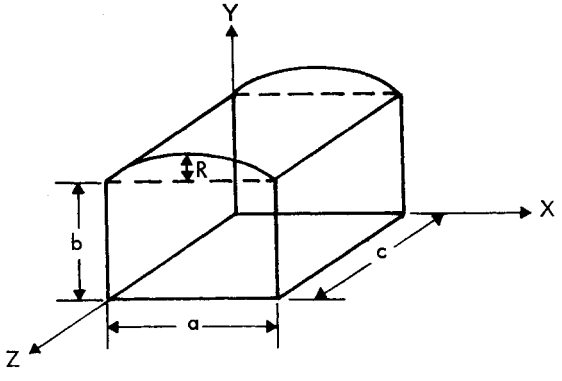

Fig. 9 Deformed parallelepiped representation for payload bay volume.

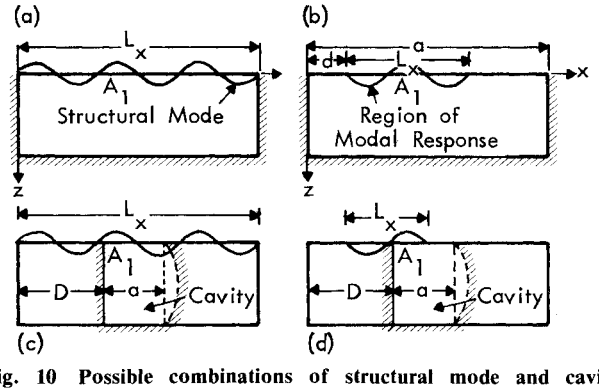

Fig. 10 Possible combinations of structural mode and cavity location.

with

$$k^{\circ}_{pqr} = \left[\left(\frac{p\pi}{a}\right)^2 + \left(\frac{q\pi}{b}\right)^2 + \left(\frac{r\pi}{b}\right)^2\right]^{1/2}$$

where k°_{pqr} is the eigenvalue of the basic rectangular parallelepiped. Also,

$$\gamma_{pq} = \frac{-\frac{2q^2\pi^2}{b^2}\left(\frac{1}{3} - \frac{1}{p^2\pi^2}\right) - \frac{4}{a^2}}{\left(\frac{p\pi}{a}\right)^2 + \left(\frac{q\pi}{b}\right)^2} \qquad (p,q>0)$$

$$\gamma_{pq} = \frac{-\frac{2q^2\pi^2}{b^2}\left(\frac{2}{3}\right) - \frac{4}{a^2}}{\left(\frac{p\pi}{a}\right)^2 + \left(\frac{q\pi}{b}\right)^2} \qquad (p=0, \quad q>0)$$

$$\gamma_{pq} = 0 \qquad (p>0, \quad q=0)$$

Similar equations can be obtained for cavities with other surfaces curved.

Returning to the coupling factor $f(n,r)$ of Eq. (4), there are several cases to be considered, four of which are sketched in Fig. 10. The simplest case is shown in Fig. 10a where the cavity is formed by the empty bay and the region of significant structural modal response extends over the full length of the cavity. For this configuration, letting $\kappa = k_p L_x/\pi$,

$$f_x(p,M) = \frac{1}{2\pi}\left[\frac{1-\cos(M-\kappa)\pi}{M-\kappa} + \frac{1-\cos(M+\kappa)\pi}{M+\kappa}\right] \qquad (k_M \neq k_p)$$

$$= 0 \qquad (k_M = k_p)$$

Power Flow into Cavity

The preceding sections have summarized the elements of the acoustic power flow model, and the main equations are presented in the Appendix. The analysis is applied separately to each of the structural regions appropriate to a given volume. The contributions are then summed to obtain the total power flow into the volume. As an example, the total calculated power flow into the empty bay is shown in Fig. 11 together with the contributions associated with resonant and nonresonant transmission through the payload bay door. Calculations of power flow to nonresonant acoustic modes are performed only at low frequencies where there is a sparsity of resonant acoustic modes. At higher frequencies, resonant acoustic response will dominate. The calculations indicate (Fig. 11) that, over a fairly wide frequency range, the door forms the dominant acoustic transmission path.

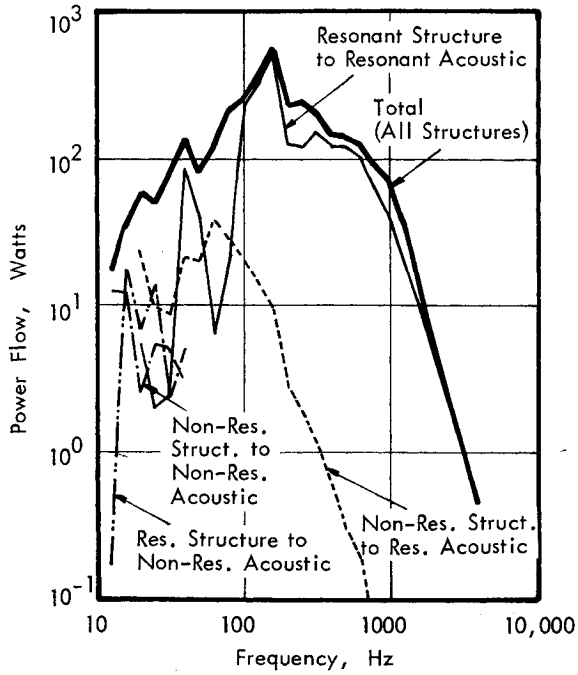

Fig. 11 Calculated power flow through payload bay door.

Power Dissipation

The acoustic power dissipated within a subvolume is determined by the energy absorbed at the surfaces of the subvolume—either by the payload bay structure, thermal control system (TCS) material, or payload structure. The time-averaged power lost by resonant acoustic modes can be written[9] in terms of the band-limited, space-averaged mean-square modal pressure $\langle p_n^2 \rangle$ in a subvolume V as

$$W_d = \frac{V}{\rho c_0^2} \sum_{n \in \Delta\omega} \frac{\eta_n \omega_n^2}{\omega} \langle p_n^2 \rangle \simeq \frac{V}{\rho c_0^2} \omega \bar{\eta}_n \langle p_l^2 \rangle \qquad (5)$$

The latter result is obtained by letting the modal acoustic loss factor η_n be approximated by the band-averaged value $\bar{\eta}_n$, and the resonance frequency ω_n by the band center frequency ω. Similar relationships exist for acoustic modes which have resonance frequencies above or below the frequency band $\Delta\omega$.[9]

At sufficiently high frequencies, the band-averaged acoustic loss factor $\bar{\eta}_n$ can be expressed in terms of the band-averaged surface acoustic absorption coefficient $\bar{\alpha}$ by means of the relationship

$$\bar{\eta}_n = c_0 A_i \bar{\alpha} / 4\omega V$$

where A_i is the area of the interior surfaces providing absorption. Values of the absorption coefficient were obtained from test data for spacecraft structures, TCS material used in the payload bay, and other sound-absorbing materials. The resulting absorption coefficient spectra are shown in Fig. 12, where the different curves associated with TCS material refer to different installation configurations.

Power Flow between Subvolumes

When there is a payload in the bay, the remaining space can be divided into a series of interconnected subvolumes. Acoustic power will then flow from one subvolume to another. For the case of resonant acoustic response, it is assumed that energy from modes resonant in a given frequency band in one subvolume is accepted in an adjoining subvolume by modes resonant in the same frequency band. Then, the net transfer of power can be written as[11]

$$W_t = \frac{A_c}{2\rho c_0}\left(\frac{\theta}{\theta^2+\chi^2}\right)(\langle p_1^2 \rangle - \langle p_2^2 \rangle)\Gamma_\epsilon \qquad (6)$$

where $\langle p_1^2 \rangle$, $\langle p_2^2 \rangle$ are the band-limited, space-averaged mean-square pressures in the two subvolumes, and the connecting opening has area A_c and impedance $(\theta - i\chi)$. Γ_ϵ is a weighting function which accounts for the relative participation of

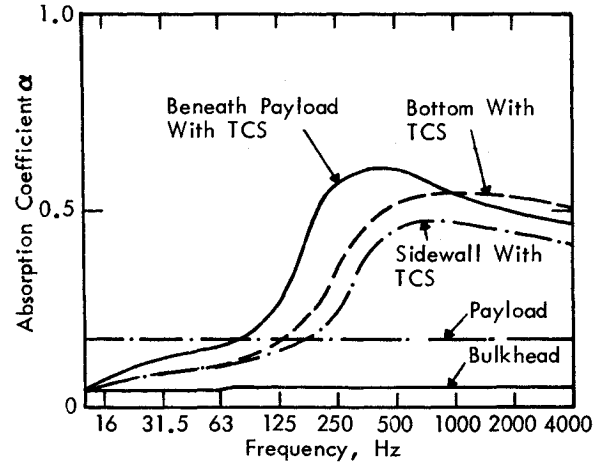

Fig. 12 Acoustic absorption coefficients for payload bay.

different modes. The coefficient of $\langle p_1^2 \rangle$ in Eq. (6) corresponds to $C_L(K,K)$ in Eq. (2), and that of $\langle p_2^2 \rangle$ to $C_L(K,I)$ in Eq. (3).

The impedance of an opening can be represented, to sufficient accuracy, by impedance functions for rectangular or circular pistons. Circular pistons are used to represent circular or large irregular openings, whereas rectangular pistons represent rectangular or slit openings. Simplified forms for resistance θ and reactance χ are given in Ref. 11.

Payload Idealization

The analytical model assumes that all surfaces of a cavity are capable of supporting standing waves. The coupling between a subvolume and the structure can then be considered in isolation from the remainder of the bay. Thus, the main task in describing the space around a payload is concerned with the definition of a series of subvolumes with reflecting surfaces. A subdivision of this type is not always possible, particularly if there are annular spaces surrounding large-diameter sections of a payload. For illustration purposes, an idealization for the Spacelab configuration 2 payload is shown in Fig. 2. Subvolumes are identified by bold numbers, and transmitting openings between subvolumes are identified by encircled numbers and zigzag lines.

The Spacelab payload consists of the access tunnel, a cylindrical module, and three pallets, one of which carries an experiment package. The payload extends for the full 18.4-m length of the bay, and displaces about 19% of the payload bay volume. In the idealization shown in Fig. 2, subvolumes 1 and 5 are separated by the cylindrical module, and subvolumes 4 and 5 are separated by the package. All three subvolumes are exposed to the payload bay door. Subvolumes 2 and 3 lie beneath the cylindrical module and the pallets, respectively. There is no strong reflecting surface between subvolumes 2 and 3, but this deviation from the criterion for selecting subvolumes does not have a significant impact on the resulting estimates of space-averaged sound pressure levels. Finally, the space (subvolume 6) around the experimental package and the annulus (subvolume 7) around the cylindrical module are referred to as "irregular" subvolumes, since they are treated rather differently from the other "regular" subvolumes.

Power flow into all subvolumes at high frequencies is calculated using Eq. (A3). Equations (A1) and (A2) are used at low frequencies except for irregular subvolumes, for which model tests indicate that reasonable estimates can be obtained using Eq. (A1) provided that frequency bands containing the lower-order modes are excluded. Finally, for the 12.5- and 16-Hz bands, the model represents the payload bay as a single unit with volume displaced by the payload. The distribution of acoustic power between the subvolumes is then assumed to be proportional to the structure transmitting areas exposed to each of the subvolumes.

Validation of Analytical Model

Validation of the analytical model has been performed for both the empty bay and the bay with payload.[2,12] In the case of the empty bay, two acoustic tests were performed on the orbiter vehicle OV 101 using either loudspeakers or jet exhausts as noise sources. Tests with a payload present involved the use of model scale payload bays and payloads.

Results from the empty bay tests with jet exhaust noise sources are shown in Fig. 13, where good agreement is found between measured and predicted interior sound levels. Typical results from one-quarter scale model tests are shown in Fig. 14 in terms of the change in payload bay sound level when the Spacelab configuration 2 payload is introduced into the bay. In most cases, the predicted change in sound level lies within the 99% confidence intervals.

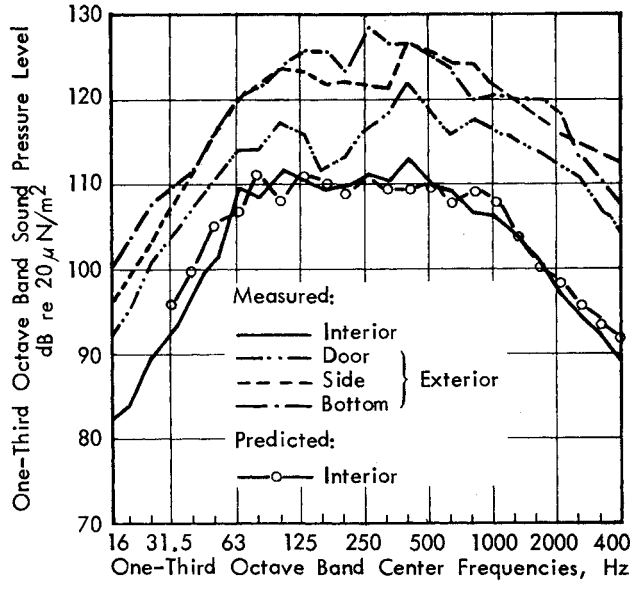

Fig. 13 Measured interior and exterior space-averaged sound levels and predicted interior levels for OV 101 jet noise tests.

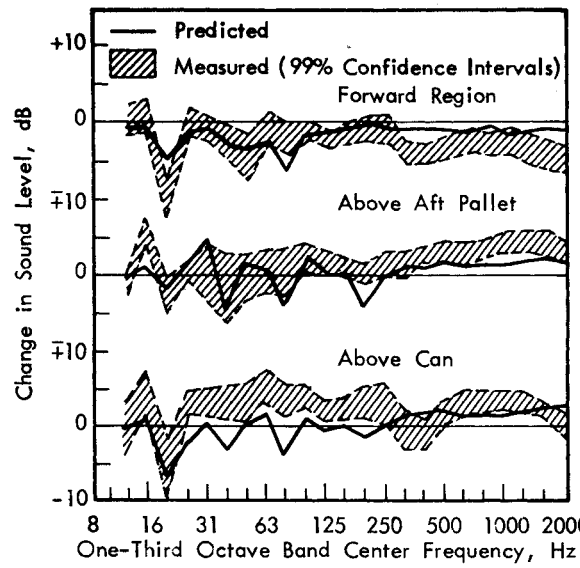

Fig. 14 Comparison of predicted and measured changes in sound levels when Spacelab payload placed in bay (one-quarter scale model).

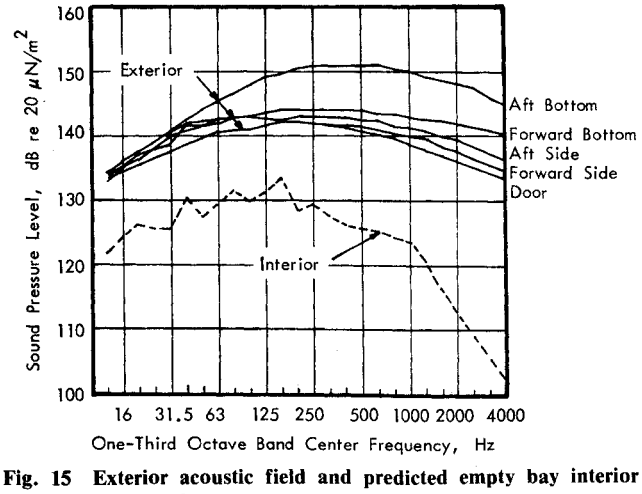

Fig. 15 Exterior acoustic field and predicted empty bay interior sound levels at liftoff.

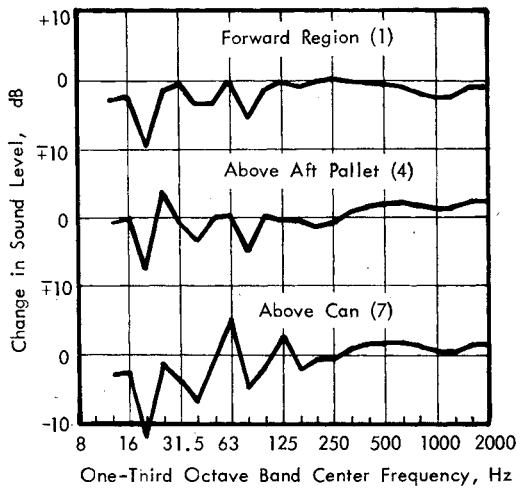

Fig. 16 Predicted change in sound level when Spacelab payload placed in bay.

Payload Bay Calculated Sound Levels

The analytical model has been used to calculate the space-averaged one-third-octave-band sound pressure levels in the empty payload bay at liftoff, using the exterior levels [12] shown in Fig. 15. The predicted interior spectrum is also shown in the figure.

When a payload is introduced, the calculated sound levels increase at some frequenies and decrease at others. As an example, Fig. 16 shows predicted changes in sound level for three subvolumes associated with the Spacelab payload idealization shown in Fig. 2. In the mid- and high-frequency ranges, the model predicts changes of up to ± 3 dB with the changes showing little variation from frequency to frequency for a given subvolume. The low-frequency range is the most interesting regime in Fig. 16 as the predictions show large changes in sound level when the payload is introduced. Furthermore, the changes vary rapidly from frequency band to frequency band, a phenomenon which can be seen in the validation test data in Fig. 14.

Concluding Remarks

The program to develop an analytical model to predict the acoustical environment in the payload bay of the Space Shuttle orbiter vehicle at liftoff has resulted in a comprehensive procedure with extensive validation. In its final form, the model should provide a reliable prediction method which can be readily adapted to other exterior pressure fields such as that of the turbulent boundary layer during ascent and re-entry. Furthermore, the general approach followed in the model should have application to a wide range of interior noise problems in aerospace vehicles.

Appendix: Power Flow Equations

Acoustic power flow equations have been developed for high- and low-frequency resonant acoustic response, [8] and for low-frequency nonresonant response. [9] The resulting equations are given in the following paragraphs so that the relevant terms can be identified.

Many of the terms contained in the equations are defined in the main text; others are defined here. The summations are performed for structural modes resonant below ($r<\Delta\omega$) and within ($r\epsilon\Delta\omega$) the frequency band $\Delta\omega$ of interest, and for acoustic modes resonant below ($n<\Delta\omega$), within ($n\epsilon\Delta\omega$), and above ($n>\Delta\omega$) the band. Structural modes resonant above the frequency band of interest are excluded since the power inflow is negligible. $\langle p_b^2\rangle$ and $\langle p_i^2\rangle$ are, respectively, the band-limited mean-square exterior blocked pressure and interior induced space-averaged pressure. The modal mass of the structure is denoted by M_r, and $\bar{\eta}_r$ denotes the sum of the structural dissipative and external radiation loss factors. The mass-law transmission coefficient for the structure is τ. The internal-looking radiation resistance is given by R_{rad}, and $j_r^2(\omega)_R$ is the structural joint acceptance function for reverberant excitation. $\langle\cdot\rangle_r$ indicates an average over all structural modes r resonant in the band $\Delta\omega$.

Low-Frequency Formulation (for one-third octave bands containing seven or less acoustic modes)

Power inflow to acoustic modes resonant in the band, from structural modes resonant below and in the band:

$$W_{in}=\frac{\langle p_b^2\rangle}{\Delta\omega}\frac{2\pi A^2}{\rho V}\left(\frac{mA}{4}\right)^2\tau\left\{\sum_{n\epsilon\Delta\omega}\epsilon_n\times\left[\sum_{r<\Delta\omega}\frac{\omega_n^4 j_r^2(\omega)f^2(n,r)}{M_r^2[(\omega_n^2-\omega_r^2)^2+\bar{\eta}_r^2\omega_r^4]}+\frac{\bar{\eta}_r+\bar{\eta}_n}{\bar{\eta}_r}\sum_{r\epsilon\Delta\omega}\frac{\omega_n^4 j_r^2(\omega)f^2(n,r)}{M_r^2[(\omega_n^2-\omega_r^2)^2+(\bar{\eta}_r+\bar{\eta}_n)^2\omega_n^4]}\right]\right\} \tag{A1}$$

Power inflow to acoustic modes resonant below and above the band, from structural modes resonant below and in the band:

$$W_{in}=\frac{\langle p_b^2\rangle}{\Delta\omega}\frac{2\pi A^2}{\rho V}\left(\frac{mA}{4}\right)^2\tau\sum_{n\notin\Delta\omega}\epsilon_n\eta_n\sum_{\substack{r<\Delta\omega\\ r\epsilon\Delta\omega}}\frac{j_r^2(\omega)f^2(n,r)}{M_r^2}\left\{\frac{2}{\pi}\frac{\omega^2\omega_n^2}{D_{nr}}\left\{\left(\frac{c_r-c_n}{4}\right)\ell n_n+\left[\frac{2c_n(b_r-b_n)-b_n(c_r-c_n)}{4\eta_n\omega_n^2}\right]\arctan_n+\left(\frac{c_n-c_r}{4}\right)\ell n_r+\left[\frac{2c_r(b_n-b_r)-b_r(c_n-c_r)}{4\eta_r\omega_r^2}\right]\arctan_r\right\}\right\} \tag{A2}$$

where

$$D_{nr}=(c_r-c_n)^2+(b_n-b_r)(b_nc_r-b_rc_n)$$

with

$$b_n=-2\omega_n^2 \qquad b_r=-2\omega_r^2 \qquad c_n=\omega_n^4(1+\eta_n^2) \qquad c_r=\omega_r^4(1+\eta_r^2)$$

and for n or $r=j$, with $c_\omega=\Delta\omega/\omega$.

$$\ell n_j=\ell n\left\{\frac{|(1+c_\omega/2)^4\omega^4+b_j(1+c_\omega/2)^2\omega^2+c_j|}{|(1-c_\omega/2)^4\omega^4+b_j(1-c_\omega/2)^2\omega^2+c_j|}\right\}$$

$$\arctan_j=\tan^{-1}\{[(2+c_\omega)^2\omega^2-4\omega_j^2]/4\eta_j\omega_j^2\}-\tan^{-1}\{[(2-c_\omega)^2\omega^2-4\omega_j^2]/4\eta_j\omega_j^2\}$$

High-Frequency Formulation (for one-third octave bands containing more than seven acoustic modes)

Net power flow to acoustic modes resonant in the band, from structural modes resonant below and in the band:

$$W=\frac{A^4}{4\pi}\frac{\rho}{c}\left[\langle p_b^2\rangle\sum_{r<\Delta\omega}\frac{j_r^2(\omega)j_r^2(\omega)_R}{M_r^2}-2\langle p_i^2\rangle\sum_{r<\Delta\omega}\frac{[j_r^2(\omega)_R]^2}{M_r^2}\right]+\frac{\pi}{2}n_rR_{\text{rad}}\left[\frac{\langle p_b^2\rangle}{4\omega\bar{\eta}_r}A^2\langle j_r^2(\omega)/M_r^2\rangle_r-\frac{\pi c}{\rho\omega^2}\langle p_i^2\rangle\langle M_r^{-1}\rangle_r\right] \tag{A3}$$

Acknowledgments

The development of the analytical model was performed under NASA Goddard Space Flight Center Contract NAS5-22832, and the authors wish to acknowledge the support given by J.P. Young, the technical monitor. The authors also wish to thank their colleagues at Bolt Beranek and Newman Inc. for their assistance at various stages of the program.

References

[1] On, F.J., "Shuttle Orbiter Payload Bay Internal Acoustic Environment During Lift-Off," NASA Goddard Space Flight Center, Rept. X-321-75-116, May 1975.

[2] Wilby, J.F. and Pope, L.D., "The Development of a Method for Predicting the Noise Exposure of Payloads in the Space Shuttle Orbiter Vehicle," *The Shock and Vibration Bulletin,* No. 49, Part 1, Sept. 1979, pp. 5-30.

[3] Hay, J.A., "Problems of Cabin Noise Estimation for Supersonic Transports," *Journal of Sound and Vibration,* Vol. 1, April 1964, pp. 113-126.

[4] Cockburn, J.A. and Jolly, A.C., "Structural-Acoustic Response, Noise Transmission Losses and Interior Noise Levels of an Airplane Fuselage Excited by Random Pressure Fields," AFFDL-TR-68-2, Aug. 1968.

[5] Wilby, J.F. and Scharton, T.D., "Acoustic Transmission through a Fuselage Sidewall," NASA CR-132602, July 1974.

[6] Koval, L., "Effects of Cavity Resonances on Sound Transmission into a Thin Cylindrical Shell," *Journal of Sound and Vibration,* Vol. 59, July 1978, pp. 23-33.

[7] Koval, L., "Effects of Longitudinal Stringers on Sound Transmission into a Thin Cylindrical Shell," *Journal of Aircraft,* Vol. 15, Dec. 1978, pp. 816-821.

[8] Pope, L.D. and Wilby, J.F., "Band-Limited Power Flow into Enclosures," *Journal Acoustical Society of America,* Vol. 62, Oct. 1977, pp. 906-911.

[9] Pope, L.D. and Wilby, J.F., "Band-Limited Power Flow into Enclosures, II," *Journal Acoustical Society of America,* Vol. 67, March 1980, pp. 823-826.

[10] Guest, S.H. and Jones, J.H., "Space Shuttle Noise Suppression Concepts for the Eastern Test Range," *Proceedings of the 13th Space Congress,* Cocoa Beach, Fla., April 1976.

[11] Pope, L.D. and Wilby, J.F., "Space Shuttle Payload Bay Acoustics Prediction Study, Analytical Model," Vol. II, NASA CR-159956, March 1980.

[12] Piersol, A.G. and Rentz, P.E., "Experimental Studies of the Space Shuttle Payload Acoustic Environment," SAE Paper 770973, Society of Automotive Engineers, Nov. 1977.